





High-energy-resolution measurements of an ultracold-atom-ion collisional cross section

Ruti Ben-shlomi ^{*}, Meirav Pinkas, Ziv Meir [†], Tomas Sikorsky [‡], Or Katz, Nitzan Akerman, and Roei Ozeri
Department of Physics of Complex Systems, Weizmann Institute of Science, Rehovot 7610001, Israel

 (Received 19 October 2020; accepted 9 February 2021; published 5 March 2021)

The cross section of a given process fundamentally quantifies the probability for that process to occur. In the quantum regime of low energies, the cross section can greatly vary with collision energy due to quantum effects. Here, we report on a method to directly measure the atom-ion collisional cross section in the energy range of $0.2\text{--}12\text{ mK} \times k_B$, by shuttling ultracold atoms trapped in an optical-lattice across a radio-frequency trapped ion. Using this method, the average number of atom-ion collisions per experiment is below one, such that the energy resolution is not limited by the broad (power-law) steady-state atom-ion energy distribution. Here, we estimate that the energy resolution is below $200\text{ }\mu\text{K} \times k_B$, limited by drifts in the ion's excess micromotion compensation and can be reduced to the tens of $\mu\text{K} \times k_B$ regime. This resolution is one order-of-magnitude better than previous experiments measuring cold atom-ion collisional cross-section energy dependence. We used our method to measure the energy dependence of the inelastic collision cross sections of a nonadiabatic electronic-excitation-exchange (EEE) and spin-orbit change (SOC) processes. We found that, in the measured energy range, the EEE and SOC cross sections statistically agree with the classical Langevin cross section. This method allows for measuring the cross sections of various inelastic processes and opens the possibility to search for atom-ion quantum signatures such as shape resonances.

DOI: [10.1103/PhysRevA.103.032805](https://doi.org/10.1103/PhysRevA.103.032805)

I. INTRODUCTION

The last decade has seen the emergence and growth of ultracold atom-ion systems. These systems have gained large interest due to their potential contribution to quantum chemistry [1–4], quantum computing [5,6], and quantum simulation [7,8] fields.

Collisions between atoms and ions are characterized by an attractive long-range polarization-potential which scales as $-r^{-4}$ which then leads to a semiclassical behavior over a wide range of collision energies [9]. At very low energies, quantum phenomena, such as Feshbach [10–12] and shape resonances [13–16], are predicted, similar to those observed in atom-atom [17] and atom-molecule [18] collisions. Therefore, considerable experimental effort is expanded for cooling atom-ion mixtures into a few-partial-wave regime, thereby measuring with high resolution the cross section's energy dependence for different collisions and reactions.

Reaching the few-partial-wave regime in atom-ion systems has been a significant challenge for the atom-ion community in the last couple of decades, the reason being that, at steady-state, the collision energy between atoms and ions is neither fundamentally limited by the temperature to which both species are cooled, nor by the trapped ion's residual excess-micromotion (EMM) energy. Instead, this fundamen-

tal limit is set by the force that the atom exerts on the ion during a collision. This force is then amplified by the ion-trap oscillating fields [19–22]. This effect sets the lower boundary of atom-ion steady-state interaction energy in these systems. Until recently, this lower boundary has been at least two orders of magnitude higher than the *s*-wave energy limit [23]. However, this fundamental energy limit is species dependent [19], and favorable for mixtures of light-atoms and heavy-ions such as ${}^6\text{Li}\text{-Yb}^+$. Researchers have only recently reached the *s*-wave regime for this system, with collisional energies of about $10\text{ }\mu\text{K} \times k_B$ [22].

In recent years, several experiments have been conducted to study the rates and cross sections of inelastic atom-ion collisions as a function of collision energy. Several experiments reached the energy regime where quantum resonances should appear [9,24–27], but they have yet to be observed. In all previous studies, scanning the energy was accompanied by increased energy spread, thereby compromising the energy resolution. One method varied the collision energies by increasing the ions' micromotion energy, which is associated with their motion in the oscillating rf electric field [24–26,28–30]. However, increasing micromotion broadened the ion energy spread into a power-law distribution, in which the distribution spread was larger than the distribution peak [13,25,31–33]. In a different experiment, a magneto-optical trap of atoms was shuttled across a crystal of atomic [34] or molecular ions [27], using radiation-pressure forces, and reaching an energy resolution in the mK regime. Another approach is shuttling the ion by modulating the voltage on the trap electrodes [35]. These methods allow the collision energy to be scanned between $\approx 10\text{ mK}$ to $\approx 1\text{ K}$ with a relative resolution of ≈ 10 . In the method presented here, the inferred

^{*}ruti.ben-shlomi@weizmann.ac.il

[†]Present address: Department of Chemistry, University of Basel, Klingelbergstrasse 80, CH-4056 Basel, Switzerland.

[‡]Present address: Atominstytut - E141, Technische Universität Wien, Stadionallee 2, 1020 Vienna, Austria.

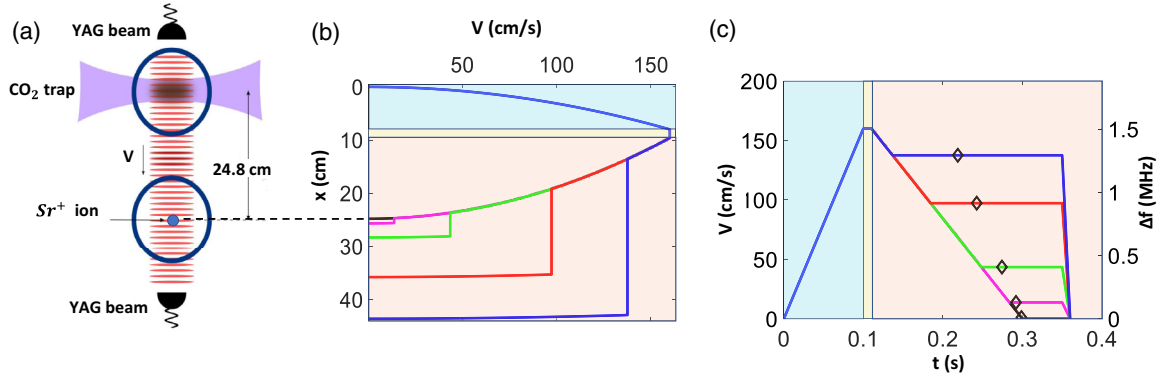


FIG. 1. An illustration of the atom-ion system and the velocity profiles of the transport. (a) The experimental setup. Rb atoms are held in a CO₂ dipole trap, loaded onto the 1D optical lattice made of two counterpropagating beams. The atoms occupy ≈ 40 lattice sites. The distance between the loading position of the atoms in the upper chamber and the ion in the lower chamber is 24.8 cm, as indicated by the dotted black curve. The figure is not to scale. (b) The atoms' position as a function of their velocity, for five different collision energies: 0, 0.1, 1, 5, and 10 $k_B \times \text{mK}$ (from black to blue and from left to right). The background represents the different stages of transport: acceleration (top, pale blue), movement in a constant velocity (middle, yellow) and deceleration to the desired collision velocity (bottom, pink). The atoms continued to be transported by the lattice at a constant velocity, even after colliding with the ion. (c) The atoms' velocity profile. The right y axis, Δf , is the frequency difference between the two lattice AOMs. The diamond indicates the times for which the atoms collide with the ion for each velocity profile.

energy resolution of $\approx 200 \mu\text{K} \times k_B$ is at least one order of magnitude narrower.

Here, we present a method for high-energy-resolution control of atom-ion collisions by shuttling a cloud of ultracold atoms, trapped in a one-dimensional optical lattice, across a single trapped ion while maintaining a narrow collision energy spread. The collision energy is scanned in a high resolution by changing the frequency difference between the optical lattice beams. We avoid the limitations imposed by the steady-state atom-ion energy distribution by limiting the average number of Langevin collisions in each pass to be smaller than one. Thus, the broadness of the collision energy is determined by the ion's and atoms' energy distributions prior to the collision, both of which are in the tens of $\mu\text{K} \times k_B$ regime. This method has sufficient energy resolution to potentially allow the observation of quantum signatures such as shape resonances.

We demonstrated our method by measuring the energy dependence of the inelastic collisions' cross sections of the electronic-excitation exchange (EEE) and spin-orbit change (SOC). These channels occur when a $^{88}\text{Sr}^+$ ion, optically excited to the $4d^2D_{5/2}$ metastable state, collides with ground-state ^{87}Rb atoms. These processes were shown [36] to occur through a nonadiabatic Landau-Zener crossing and their energy dependence was only theoretically discussed up to now [16,37] for the same collisional energy range. We measured the energy dependence of the inelastic collision's cross section of the EEE channel and the SOC channels separately. We found that, for collision energies in the range 0.2–12 $\text{mK} \times k_B$, the cross section for both channels follows the semiclassical Langevin $E^{-1/2}$ scaling with good statistical significance.

Finally, we discuss in this paper the effect of multiple collisions on the energy resolution of our method and also analyze possible deviations from the semiclassical Langevin scaling, in search of quantum resonances, by performing a maximum-likelihood estimation test.

II. EXPERIMENTAL SETUP

An illustration of our experimental setup is shown in Fig. 1. Our hybrid atom-ion system is described in detail in another article [38]. The setup consists of two separate vacuum chambers. In the top chamber, $\approx 5 \times 10^7$ cold Rb atoms were trapped in a magneto-optical-trap and then loaded into a CO₂ trap to evaporatively cool the atoms to the $\approx 5 \mu\text{K} \times k_B$ temperature range. At the end of the evaporation, $\approx 50\,000$ atoms remained in the CO₂ trap and were adiabatically loaded into a one-dimensional (1D) optical lattice. The lattice consists of two counterpropagating YAG laser beams ($\lambda = 1064 \text{ nm}$, $P = 1.5$ watts for each beam), which are collimated, vertically orientated, and have a Gaussian profile [39]. The beams are characterized by a waist of $\approx 220 \mu\text{m}$ and a Rayleigh range of $z_R = \pi w_0^2/\lambda = 143 \text{ mm}$, comparable to the transport distance to the bottom chamber of 248 mm. The strong confinement of the atoms in the optical lattice sites in the transport direction prevented the loss of atoms due to gravity. The atoms were then shuttled to the bottom chamber by changing the relative frequency between the two lattice beams (further details in the next section). During the transport, a $^{88}\text{Sr}^+$ ion was held in a linear segmented rf Paul trap, optically pumped to a specific Zeeman state in the electronic ground state, $5s^2S_{1/2}$ ($m = -1/2$), followed by ground-state cooling on all three motional modes to $\bar{n} < 0.1$. To avoid EMM drifts, the EMM was repeatedly compensated approximately every half hour throughout the experiment.

After conducting a thorough analysis of the EMM in our system, the sum of all EMM contributions was found to be $\approx 30 \mu\text{K} \times k_B$ [38]. This number can be used to estimate the energy resolution's lower boundary of this method in our system. Here, however, due to drifts in the micromotion compensation during the experiment, we set the EMM's upper limit in our system to be $\approx 200 \mu\text{K} \times k_B$, which sets the limit for the resolution in the experiments presented here.

III. COLLISION VELOCITY CONTROL

We set the relative velocity of the atoms compared with the stationary ion by controlling the relative frequency of the lattice beams. The atoms' velocity was directly proportional to the instantaneous frequency differences between the beams, $\Delta f(t)$, and equal to $v(t) = \frac{\lambda \Delta f(t)}{2}$ in the lab frame, where $\lambda = 1064$ nm is the laser wavelength. The linear velocity of the atoms in the lattice was much higher than the thermal velocity of the atoms or the ion. Therefore, the atom-ion collision energy is set by the velocity of the lattice. To transport the cloud of atoms across the trapped-ion in a well-defined collision energy, $E_{\text{coll}} = \frac{1}{2}m_{\text{Rb}}v_{\text{lattice}}^2$, in the lab frame, the frequency difference between the laser beams should satisfy,

$$\Delta f(t) = 2\sqrt{(2E_{\text{coll}}/m_{\text{Rb}})/\lambda}. \quad (1)$$

Here, m_{Rb} is the mass of the Rb atom. The two lattice beams pass through separate acousto-optic modulators (AOMs) in a double-pass configuration to control their frequency and intensity. After the AOMs, the beams are coupled to fibers, one entering from above the atom chamber and the other from below the ion chamber, as illustrated in Fig. 1(a). When varying the AOM's frequency, different diffraction angles cause a change in the intensity of the beams. Therefore, we actively stabilized the intensity level of each beam, maintaining a constant intensity throughout the entire experiment. Each lattice beam is connected to a separate frequency channel of a function-generator capable of generating a trapezoidal sweep of the frequency independently in each channel. The two trapezoidal sweeps combined to generate the relative frequency profile $\Delta f(t)$, shown in Fig. 1(c). (see Appendix).

To bring the atoms to the desired velocity when colliding with the ion, the frequencies of both lattice beams were controlled. The frequency profile was designed so that the atoms will always accelerate to the same maximal velocity and then decelerate to the desirable collision velocity, as can be seen in Figs. 1(b) and 1(c). The atoms reached a maximal velocity of $v = 160$ cm/s after 0.1 s of acceleration. The atoms were then held at a constant velocity for 0.01 s, and afterwards decelerated to the desired velocity. By using this velocity regime, the transport itself involved negligible atom loss, whereas higher velocities would introduce losses.

The distance traveled by the atoms as a function of their instantaneous velocity is shown in Fig. 1(b) for different transport profiles. After the first 0.11 s, the atoms were transported 9.6 cm. From this point, the atoms decelerated until the desired velocity was reached. For each collision energy, the atoms stopped decelerating at different positions relative to the ion. The atoms continued to move at a constant velocity until they passed the ion's position.

IV. MEASURING INELASTIC COLLISIONAL CROSS SECTIONS

The rate at which a given inelastic collision occurs is given by

$$\Gamma_{\text{inelastic}} = n_{\text{atoms}}\sigma(E_{\text{coll}})v_{\text{coll}}, \quad (2)$$

where n_{atoms} is the atomic density, $\sigma(E_{\text{coll}})$ is the inelastic collisional cross section, which is energy dependent, and v_{coll} is the relative atom-ion velocity in the center-of-mass frame.

In the proposed scheme, the atomic density in the ion's position is time-dependent due to the relative motion of the atoms in the lattice with respect to the stationary ion. The mean number of collisions per pass is given by

$$N = \sigma(E_{\text{coll}})v_{\text{coll}} \int_{-\infty}^{+\infty} n_{\text{atoms}}(t)dt. \quad (3)$$

Since the atoms move at a constant velocity v_{lattice} , the integration can be taken over a spatial dimension, in the moving direction of the lattice,

$$N = \sigma(E_{\text{coll}}) \frac{v_{\text{coll}}}{v_{\text{lattice}}} \int_{-\infty}^{+\infty} n_{\text{atoms}}(x)dx. \quad (4)$$

Here, the temperatures of the ion and atoms are negligible relative to the velocity of the atoms in the lattice, and since the ion is stationary, this collision velocity is equal to the lattice velocity $v_{\text{coll}} = v_{\text{lattice}}$, in the lab frame. The number of collisions per pass is

$$N = \sigma(E_{\text{coll}}) \int_{-\infty}^{+\infty} n_{\text{atoms}}(x)dx. \quad (5)$$

Therefore, the number of events we measure is directly proportional to the collisional cross section, through the density of the atoms in the lattice, integrated along the vertical direction of motion.

Assuming the length of the atomic cloud is finite, denoting it by L_{Rb} , we can rewrite the number of event as

$$N = n_{\text{eff}}L_{\text{Rb}}\sigma(E_{\text{coll}}), \quad (6)$$

where we define an effective density as

$$n_{\text{eff}} \equiv \frac{1}{L_{\text{Rb}}} \int_{-\infty}^{+\infty} n_{\text{atoms}}(x)dx. \quad (7)$$

In the semiclassical regime, the total cross section for hard-sphere collisions between an ion and an atom is given by the Langevin cross section [40]:

$$\sigma_L = \pi \sqrt{\frac{2C_4}{E_{\text{coll}}}}, \quad (8)$$

Where $C_4 = \alpha e^2 / (4\pi\epsilon_0)^2$, with α , e , and ϵ_0 being the atom's polarizability, electric charge and the vacuum permittivity, respectively.

Thus, the mean number of Langevin collisions per pass is

$$N_L = \pi n_{\text{eff}}L_{\text{Rb}} \sqrt{\frac{2C_4}{E_{\text{coll}}}}. \quad (9)$$

In the semiclassical regime, inelastic processes are proportional to the Langevin cross section and therefore scale as $\approx E_{\text{coll}}^{-1/2}$.

V. ENERGY DEPENDENCE OF NONADIABATIC QUENCH OF METASTABLE EXCITED STATES

To demonstrate our method, we measured the energy dependence of a nonadiabatic quench of an ion's metastable

electronically excited level during a collision with a ground-state atom. In previous work [36], we found that the excited long-lived $4d^2D_{5/2}$ and $4d^2D_{3/2}$ states of the $^{88}\text{Sr}^+$ ion quench after roughly three Langevin collisions with ground-state ^{87}Rb atoms, and that the excitation energy is transformed into the kinetic energy of the colliding particles.

In Ref. [36] we identified two types of collisional quenching. One is EEE, where the ion relaxes to the ground S state and the atom is excited to the P state followed by an energy release of $\approx 3000 \text{ K} \times k_B$. The second is SOC, where the ion relaxes from the higher fine-structure $D_{5/2}$ level to the lower $D_{3/2}$ level releasing $\approx 400 \text{ K} \times k_B$ into kinetic energy. These processes were theoretically understood to occur through Landau-Zener avoided crossings between the different molecular potential curves.

Here, we measured the dependency of these inelastic cross sections on the collision energy. As described above, a single Sr^+ ion, cooled to its ground-state in all three motional modes and with a residual EMM bounded by $\approx 200 \mu\text{K} \times k_B$, was prepared in the $4d^2D_{5/2}(m = -5/2)$ lower Zeeman state. Here, we report a higher boundary on the EMM value than what was reported in Ref. [38] since it was less frequently compensated due to long interrogation times. Meanwhile, a cloud of nonpolarized atoms was loaded into the optical lattice and shuttled to the lower chamber while scanning 119 energy points, from 0.2 to 12 mK in the lab frame with energy steps of $100 \mu\text{K} \times k_B$. The average number of Langevin collisions per sweep was tuned to be 0.09 in the lowest energy point.

After the atoms passed across the ion, we performed on the ion single-shot Doppler thermometry [41] to detect the quenched (hotter than \approx tens of $\text{K} \times k_B$) events from the non-quenched events. Due to the large energy separation between the SOC ($400 \text{ K} \times k_B$) and EEE ($3000 \text{ K} \times k_B$) energy release, these events are easily separated using single-shot thermometry [36]. As a control experiment, we tested whether quench events are detected in the absence of atoms in the optical lattice. Since no hot events were observed in the absence of atoms, we concluded that our measurements had no false positive detection of quench events. To avoid cumulative systematic noise, we scanned the collision's energy in a randomized manner by performing a single experiment for each energy value and only then repeating the experiment to accumulate the signal. The quench data presented in Fig. 2(a) was derived from 300 000 repetitions in which 3100 quench events were identified. The repetition time ranged from 1 to 10 s, depending on the quench channel and the Doppler-recooling time. These data was integrated over weeks.

In Fig. 2, we present our measurement results. We plotted the quench cross section as a function of the relative collisional energy through the relation of Eq. (6):

$$\sigma_{\text{Quench}}(E_{\text{coll}}) = \frac{N_{\text{Quench}}}{n_{\text{eff}}L_{\text{Rb}}}. \quad (10)$$

In this experiment, the typical, effective, atomic density is $n_{\text{eff}} = 4.4 \times 10^{17} \text{ m}^{-3}$. The collisional velocity ranged from $v_{\text{coll}} = 19.4$ to 150 cm/s , which corresponds to collision energies of 0.2 to $12 \text{ mK} \times k_B$, respectively. The size of the cloud in the transport direction is $L_{\text{Rb}} = 20 \mu\text{m}$, which occupies ≈ 40 lattice sites. Here, different sets of data were taken with different cloud densities, resulting in additional

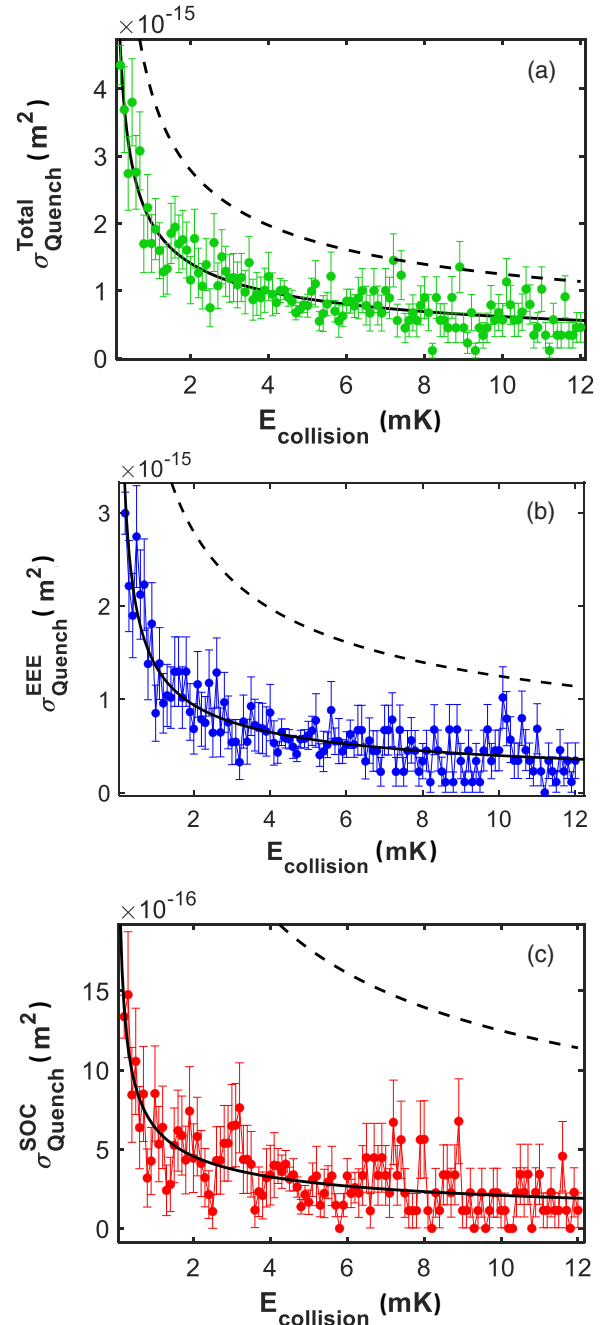


FIG. 2. Quench cross section as a function of the collision energy. (a) The total quench probability (top, green) and for the (b) EEE (middle, blue) and (c) SOC (bottom, red) channels, separately. Error bars are 1σ standard deviation of a binomial distribution and also include systematic noise, as explained in the body of the text. Smaller error bars indicate areas over which more repetitions were performed. The solid black curve is an exponential fit to AE^α , where the exponents given by the fits are $\alpha = -0.51(3)$, $-0.53(4)$, and $-0.48(6)$, respectively. The dashed black lines indicate the Langevin cross section given by Eq. (8).

systematic noise and biasing the overall data in the vertical direction on the graph. This systematic noise is estimated to be $\Delta(n_{\text{eff}}L_{\text{Rb}}) \approx 15\%$. The statistical noise, for comparison, varies between 5% to 30%, depending on the number of repetitions.

The data presented in green in Fig. 2(a) contain all quench events summing over both channels. In Figs. 2(b) and 2(c) we show the energy-dependent collisional cross section for EEE (middle, blue) and SOC (bottom, red) channels, respectively. The solid black curves are fits to a power law AE^α . The fitted power-law exponent α agrees well with the Langevin scaling of $E^{-1/2}$ (see Fig. 2 caption). Quenching from the metastable D state happens when the atom and ion reach very short internuclear distances and overcome the centrifugal barrier. Therefore, these types of collisions are Langevin collisions but happen with lower probabilities. Here we compare the cross sections through

$$\sigma_{\text{Quench}}(E_{\text{coll}}) = \eta\sigma_L(E_{\text{coll}}). \quad (11)$$

By fitting the data to Eq. (11) with η as a free parameter, we find that $\sigma_{\text{Quench}}(E_{\text{coll}})$ is proportional but smaller than the Langevin cross section by $\eta = 0.52(6)$, $0.35(5)$, and $0.16(3)$ for the green (top), blue (middle), and red (bottom) data, respectively. While this total cross section is slightly higher than those reported in previous studies [36] [0.52(6) compared with 0.38(5)], the ratio between the two channels $\sigma_{\text{Quench}}^{\text{SOC}}/\sigma_{\text{Quench}}^{\text{EEE}}$ agrees within the statistical error [0.48(11) compared with 0.39(5) in the previous measurements].

VI. THE EFFECT OF MULTIPLE COLLISIONS

In this experiment the atoms were much colder than the ion and, therefore, the energy resolution of our measurement is mainly limited by the energy uncertainty of the latter. Since the ion is cooled to the ground state of all its secular motional modes, the initial residual energy prior to the collision was mainly due to the residual EMM.

However, after a collision, the ion's energy can be changed due to coupling the EMM to the ion's external degrees of freedom [42] or due to an exchange of kinetic energy between the atom and the ion [43,44]. Both of these effects depend on the position and phase of the ion in the rf trap and lead to a power-law energy distribution [45]. Thus, in determining the energy spread of the ion before a reaction occurs, we have to take into account the possibility of the ion heating due to previous, elastic, Langevin collisions.

To find the ion's energy distribution after a certain average number of collisions, we performed a molecular-dynamics simulation which takes into account the residual EMM of the ion and the lattice velocity, as described in Refs. [38,42]. In Fig. 3, the energy distribution of the ion after a single collision is shown for different lattice velocities. As can be seen, following a single collision, the ion heats up to the energy of the moving lattice, with a wide energy distribution. As a result, if the measured inelastic process (for example, a quench) does not occur in the first collision, the collision energy is no longer defined by the velocity of the lattice and has a wide distribution.

The probability for multiple Langevin collision events can be reduced by lowering the density of atoms loaded into the lattice dipole trap. However, this leads to longer integration times. For example, in the data of Fig. 2, the probability for at least one Langevin collision per pass was approximately 0.09 for low collisional energies. For this low mean number of collisions, the probability for observing a quench event

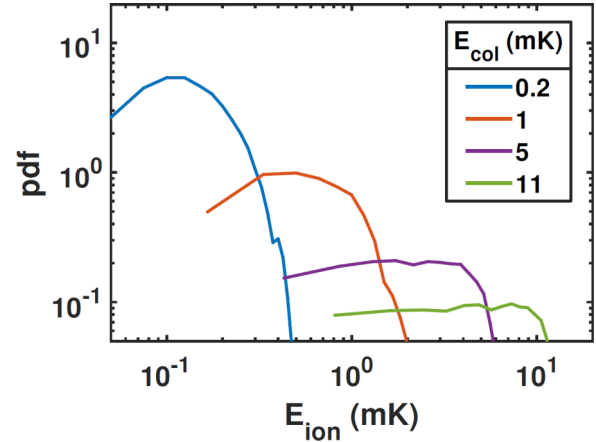


FIG. 3. (a) The distribution of the ion's energy E_{ion} after a single collision with an atom in the moving optical lattice, for different lattice velocities, E_{col} , ranging from 0.2 to 11 mK (from left to right). The distributions are calculated by a molecular-dynamics simulation that takes into account the Paul trap potential and the EMM of the ion.

that occurred in a secondary collision is $\approx 9 \times 10^{-4}$. Thus, while the fraction of quench events observed that were not the result of a first Langevin collision is finite (≈ 0.09), it is small and negligibly effects a search for narrow features. The consequential trade-off was that this measurement lasted for several weeks.

VII. A SEARCH FOR QUANTUM RESONANCES USING A MAXIMUM LIKELIHOOD ESTIMATION

A hallmark of quantum scattering in the low-energy regime is the appearance of scattering resonances. Such resonances occur, for example, when the collision energy in the center-of-mass frame resonates with the energy of a quasibound molecular state of the centrifugal barrier of one of the involved partial waves. These shape resonances are anticipated to occur in atom-ion collisions even in the mK energy range [13,15,16]. To search for such resonances, we performed a likelihood-ratio test to differentiate between the resonance and no-resonance hypotheses and calculated their statistical significance.

At each collision energy E_i the number of observed quench events is a random variable which follows a binomial distribution. The log-likelihood function for observing k_i quench events out of N repetitions is, up to a constant factor,

$$\ln \mathcal{L}(p_i | k_i, N_i) = k_i \ln p_i + (N - k_i) \ln (1 - p_i), \quad (12)$$

where p_i is the probability for observing a quench event in a single experiment.

The total log-likelihood for observing $\mathbf{k} = \{k_i\}$ quench events in all energy points is the sum over the log-likelihood function in each point,

$$\ln \mathcal{L}(\mathbf{p} | \mathbf{k}, \mathbf{N}) = \sum_i \ln \mathcal{L}(p_i | k_i, N_i). \quad (13)$$

We wanted to estimate the probability that the data we measured is the result of a local peak at some energy point.

The null hypothesis H_0 assumes that the measured data has as a power-law $p_i(E_i) = CE^{-\alpha}$ behavior, whereas the alternative hypothesis includes a Gaussian resonance at energy E_0 with a width of σ_g and magnitude A :

$$p_i = CE^{-\alpha} + Ae^{-\frac{(E_i - E_0)^2}{\sigma_g^2}}. \quad (14)$$

We estimated the free parameters (C , α , A , σ , and E_0) as the parameters that maximize the log-likelihood function for our measured data. Using these parameters, we calculated the observed likelihood-ratio between the null hypothesis and the alternative hypothesis

$$\ln \lambda_{\text{obs}} = \max \ln \mathcal{L}_0 - \max \ln \mathcal{L}_1. \quad (15)$$

To make the maximization process of the alternative hypothesis more robust, we found the maximum likelihood for a resonance separately for each energy point, and then identified the energy point that yielded the maximal likelihood as a suspect for resonance.

We used the likelihood ratio of the measurement to estimate the statistical significance of the alternative hypothesis over the null hypothesis. To this end, we calculated the p value: the probability of observing a likelihood-ratio that is higher than the one we measured under the null hypothesis. A small p value indicates that it is less likely that our measured data was generated by the null hypothesis and the resonance hypothesis is favorable. The p -value can be related to the number of standard deviations, N_σ , of the observed data from the null hypothesis [46]:

$$p = 1 - \text{erf}\left(\frac{N_\sigma}{\sqrt{2}}\right), \quad (16)$$

where $\text{erf}(x)$ is the standard error function.

To find the p value of our measurement, we simulated 1000 experiments (3000 for the SOC experiment), each with the same number of repetitions that we had in the real experiment, under the null hypothesis. For each one of these simulations, we repeated the analysis above to find the likelihood ratio. From the simulated likelihood-ratio distribution we found the fraction of experiments that yielded a higher value than our observed likelihood ratio, which gives the p value of the measurement.

Analyzing the EEE events, we observed a weak resonance at 10.3 mK with a likelihood ratio of 4.6 and a p value of 0.091, equivalent to 1.7σ , see Fig. 4(a). The analysis of the SOC events [Fig. 4(b)], indicated a peak around 3 mK with a likelihood ratio of 7.9. The p value in this case is 0.0088, equivalent to 2.6σ , which is marginally significant.

Longer integration and improved statistics around suspected energies will help determine whether there is a resonance behavior. However, longer integrations can suffer from systematic drifts that will wash out the effect of a resonance. A further investigation of this effect with higher statistics is needed, with improved experimental repetition rates to avoid drifts.

VIII. CONCLUSIONS

In this work we present a method for controlling atom-ion collisional energy in the ultracold regime, with an order

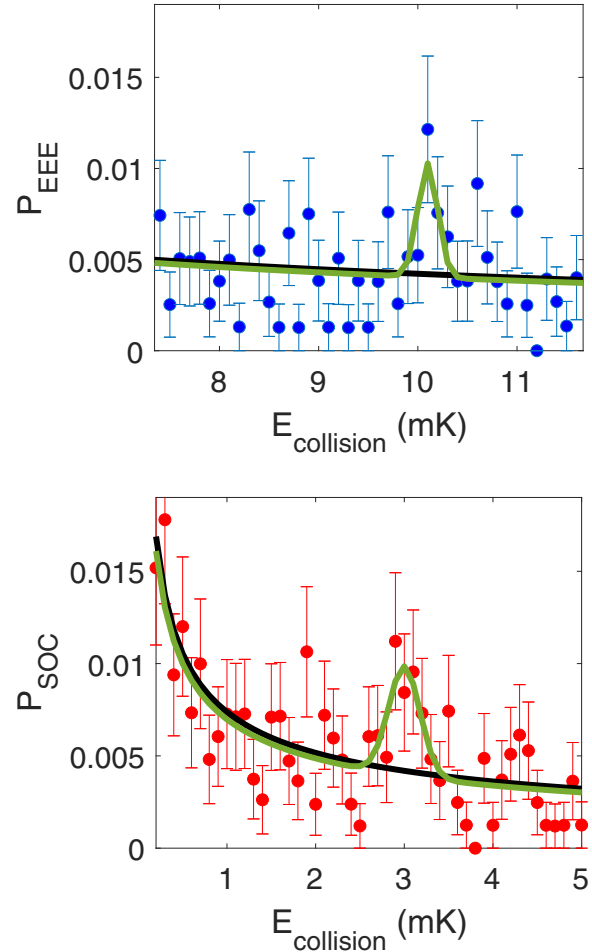


FIG. 4. Maximum likelihood estimation for a semiclassical cross section for the non-normalized, EEE channel (up) and SOC channel (down), with and without a Gaussian resonance, green (gray) and black, respectively. The p values are 0.091 and 0.0088, which correspond to 1.7σ and 2.6σ for the EEE and SOC channels, respectively.

of magnitude improved energy resolution as compared with previous methods, by optically shuttling the atoms across a single trapped-ion. The high energy resolution of the studied reactions is maintained by limiting the number of atom-ion collisions in each experimental repetition to be below one. The method is currently limited only by an EMM compensation to below $200 \mu\text{K} \times k_B$ in this experiment with the potential to reach the tens of $\mu\text{K} \times k_B$ level with better control over the EMM over long time periods.

To demonstrate our method, we used it to measure the energy dependence of the collisional quench processes of the ion from an optically excited metastable state. We found that the cross section for these processes follows the semiclassical Langevin prediction. Finally, we identified suspect energies for the possible location of a quantum resonance. Further experimental investigation is necessary to determine whether a resonance is actually present. Our method is generic and can be used for different species and for the study of different atom-ion reactions. With sufficient control of experimental

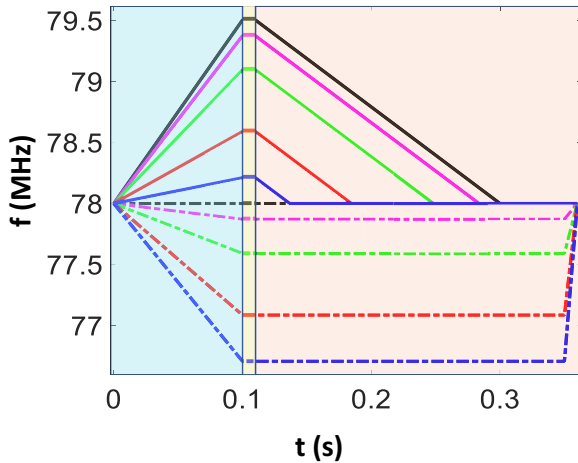


FIG. 5. The frequency profiles of the two AOMs controlling the frequency of the lattice laser beams. The solid (dotted-dashed) curve refers to the frequency set by the function-generator of the upper (and lower) lattice beam.

parameters, it can be used to measure atom-ion quantum-scattering effects in the low partial-wave regime.

ACKNOWLEDGMENTS

This work was supported by the Israeli Science Foundation and the Israeli Ministry of Science Technology and Space.

APPENDIX: FREQUENCY PROFILES

The trapezoidal frequency profile is characterized for each lattice beam by a start frequency f_s and an intermediate frequency f_i and three different stages: rise time in which the frequency is linearly increased from f_s to f_i ; hold time in which the frequency is kept constant at f_i ; and return time in which the frequency is linearly decreased from f_i to f_s again. To move the atoms from the upper chamber to the ion in the lower chamber such that they will stop exactly on the ion, we use a trapezoidal frequency profile on one beam only, as illustrated by the top, black solid line in Fig. 5, while keeping the second beam at a constant frequency (top, black dotted-dashed line). We accelerated the atoms downwards for 0.1 s to a velocity of 160 cm/s, then we kept them for 0.01 s under constant velocity, followed by a deceleration for 0.2 s back to rest. The start frequency of both channels that fed into both AOMs was set to $f_s = 78$ MHz. The intermediate frequencies of the two AOMs are defined as $f_i^1 = f_s + f_0 - f_f$, $f_i^2 = f_s - f_f$, where $f_0 = 1503.9$ kHz is the offset frequency corresponding to the maximal velocity of the atoms and f_f is the final given frequency reproducing the desired collisional energy:

$$f_f = \Delta f(t)/2 = \sqrt{(2E_{\text{coll}}/m_{\text{Rb}})}/\lambda, \quad (\text{A1})$$

where the factor of two is due to the double-pass AOMs configuration. Note that, for the second AOM, the hold time is longer than the time it takes the atoms to reach the ion to reach the correct final velocity.

- [1] L. Ratschbacher, C. Zipkes, C. Sias, and M. Köhl, *Nat. Phys.* **8**, 649 (2012).
- [2] P. Puri, M. Mills, C. Schneider, I. Simbotin, J. A. Montgomery Jr., R. Côté, A. G. Suits, and E. R. Hudson, *Science* **357**, 1370 (2017).
- [3] Y. P. Chang, K. Długołcki, J. Küpper, D. Rösch, D. Wild, and S. Willitsch, *Science* **342**, 98 (2013).
- [4] Y. P. Chang, K. Długołcki, J. Küpper, D. Rösch, D. Wild, and S. Willitsch, *Nat. Commun.* **9**, 920 (2018).
- [5] H. Doerk, Z. Idziaszek, and T. Calarco, *Phys. Rev. A* **81**, 012708 (2010).
- [6] R. Gerritsma, A. Negretti, H. Doerk, Z. Idziaszek, T. Calarco, and F. Schmidt-Kaler, *Phys. Rev. Lett.* **109**, 080402 (2012).
- [7] J. Joger, A. Negretti, and R. Gerritsma, *Phys. Rev. A* **89**, 063621 (2014).
- [8] T. Secker, R. Gerritsma, A. W. Glaetzle, and A. Negretti, *Phys. Rev. A* **94**, 013420 (2016).
- [9] R. Saito, S. Haze, M. Sasakawa, R. Nakai, M. Raoult, H. Da Silva, Jr., O. Dulieu, and T. Mukaiyama, *Phys. Rev. A* **95**, 032709 (2017).
- [10] Z. Idziaszek, T. Calarco, P. S. Julienne, and A. Simoni, *Phys. Rev. A* **79**, 010702(R) (2009).
- [11] Z. Idziaszek, A. Simoni, T. Calarco, and P. S. Julienne, *New J. Phys.* **13**, 083005 (2011).
- [12] M. Tomza, C. P. Koch, and R. Moszynski, *Phys. Rev. A* **91**, 042706 (2015).
- [13] H. da Silva Jr, M. Raoult, M. Aymar, and O. Dulieu, *New J. Phys.* **17**, 045015 (2015).
- [14] P. Raab and H. Friedrich, *Phys. Rev. A* **80**, 052705 (2009).
- [15] M. Tacconi, F. A. Gianturco, and A. K. Belyaev, *Phys. Chem. Chem. Phys.* **13**, 19156 (2011).
- [16] A. K. Belyaev, S. A. Yakovleva, M. Tacconi, and F. A. Gianturco, *Phys. Rev. A* **85**, 042716 (2012).
- [17] S. Inouye, M. R. Andrews, J. Stenger, H.-J. Miesner, D. M. Stamper-Kurn, and W. Ketterle, *Nature (London)* **392**, 151 (1998).
- [18] A. Klein, Y. Shagam, W. Skomorowski, P. S. Żuchowski, M. Pawlak, L. M. C. Janssen, N. Moiseyev, S. Y. T. van de Meerakker, A. van der Avoird, C. P. Koch, and E. Narevicius, *Nat. Phys.* **13**, 35 (2017).
- [19] M. Cetina, A. T. Grier, and V. Vuletic, *Phys. Rev. Lett.* **109**, 253201 (2012).
- [20] Z. Meir, T. Sikorsky, R. Ben-shlomi, N. Akerman, Y. Dallal, and R. Ozeri, *Phys. Rev. Lett.* **117**, 243401 (2016).
- [21] M. Pinkas, Z. Meir, T. Sikorsky, R. Ben-shlomi, N. Akerman, and R. Ozeri, *New J. Phys.* **22**, 013047 (2020).
- [22] T. Feldker, H. Fürst, H. Hirzler, N. V. Ewald, M. Mazzanti, D. Wiater, M. Tomza, and R. Gerritsma, *Nat. Phys.* **16**, 413 (2020).
- [23] T. Schmid, C. Veit, N. Zuber, R. Löw, T. Pfau, M. Tarana, and M. Tomza, *Phys. Rev. Lett.* **120**, 153401 (2018).
- [24] F. H. J. Hall, P. Eberle, G. Hegi, M. Raoult, M. Aymar, O. Dulieu, and S. Willitsch, *Mol. Phys.* **111**, 2020 (2013).
- [25] F. H. J. Hall and S. Willitsch, *Phys. Rev. Lett.* **109**, 233202 (2012).
- [26] S. Haze, S. Hata, M. Fujinaga, and T. Mukaiyama, *Phys. Rev. A* **87**, 052715 (2013).
- [27] A. D. Dörfler, P. Eberle, D. Koner, M. Tomza, M. Meuwly, and S. Willitsch, *Nat. Commun.* **10**, 5429 (2019).

- [28] C. Zipkes, S. Palzer, and M. Köhl, *Nature (London)* **464**, 388 (2010).
- [29] S. Schmid, A. Härter, and J. H. Denschlag, *Phys. Rev. Lett.* **105**, 133202 (2010).
- [30] S. Schmid, A. Härter, A. Frisch, S. Honika, and J. H. Denschlag, *Rev. Sci. Instrum.* **83**, 053108 (2012).
- [31] M. T. Bell, A. D. Gingell, J. Oldham, T. P. Softley, and S. Willitsch, *Faraday Discuss.* **142**, 73 (2009).
- [32] A. T. Grier, M. Cetina, F. Oručević, and V. Vuletić, *Phys. Rev. Lett.* **102**, 223201 (2009).
- [33] P. Puri, M. Mills, I. Simbotin, J. A. Montgomery Jr., R. Côté, C. Schneider, A. G. Suits, and E. R. Hudson, *Nat. Chem.* **11**, 615 (2019).
- [34] P. Eberle, A. D. Dörfler, C. von Planta, K. Ravi, and S. Willitsch, *ChemPhysChem* **17**, 3769 (2016).
- [35] P. Puri, M. Mills, E. P. West, C. Schneider, and E. R. Hudson, *Rev. Sci. Instrum.* **89**, 083112 (2018).
- [36] R. Ben-shlomi, R. Vexiau, Z. Meir, T. Sikorsky, N. Akerman, M. Pinkas, O. Dulieu, and R. Ozeri, *Phys. Rev. A* **102**, 031301(R) (2020).
- [37] F. H. J. Hall, M. Aymar, N. Bouloufa-Maafa, O. Dulieu, and S. Willitsch, *Phys. Rev. Lett.* **107**, 243202 (2011).
- [38] Z. Meir, T. Sikorsky, R. Ben-shlomi, N. Akerman, M. Pinkas, Y. Dallal, and R. Ozeri, *J. Mod. Opt.* **65**, 501 (2018).
- [39] S. Schmid, G. Thalhammer, K. Winkler, F. Lang, and J. H. Denschlag, *New J. Phys.* **8**, 159 (2006).
- [40] P. Langevin, *Ann. Chim. Phys.* **5**, 245 (1905).
- [41] Z. Meir, T. Sikorsky, N. Akerman, R. Ben-shlomi, M. Pinkas, and R. Ozeri, *Phys. Rev. A* **96**, 020701(R) (2017).
- [42] C. Zipkes, L. Ratschbacher, C. Sias, and M. Kohl, *New J. Phys.* **13**, 053020 (2011).
- [43] R. G. DeVoe, *Phys. Rev. Lett.* **102**, 063001 (2009).
- [44] K. Chen, S. T. Sullivan, and E. R. Hudson, *Phys. Rev. Lett.* **112**, 143009 (2014).
- [45] I. Rouse and S. Willitsch, *Phys. Rev. Lett.* **118**, 143401 (2017).
- [46] L. Demortier, CDF/MEMO/STATISTICS/PUBLIC/8662, The Collider Detector at Fermilab notes (2007), <https://www-cdf.fnal.gov/~luc/statistics/cdf8662.pdf>.